P. Masarati, G. Quaranta, L. Lu, M. Jump
A Closed Loop Experiment of Collective Bounce Aeroelastic Rotorcraft-Pilot Coupling
Journal of Sound and Vibration, Vol. 333, N. 1, 2014, p. 307-325
doi:10.1016/j.jsv.2013.09.020

A Closed Loop Experiment of Collective Bounce Aeroelastic Rotorcraft-Pilot Coupling

Pierangelo Masarati *, Giuseppe Quaranta

Dipartimento di Ingegneria Aerospaziale, Politecnico di Milano
via La Masa 34, 20156 Milano, Italy

Linghai Lu, Michael Jump

School of Engineering, The University of Liverpool
Walker Building, The Quadrangle, Liverpool L69 3GH, United Kingdom

Abstract

This work presents an experimental study that investigated the possibility of destabilising a rotorcraft by coupling the biomechanical behaviour of human subjects with the dynamics of the vehicle. The results of a study focused on the behaviour of pilots holding the collective control inceptor in a flight simulator are discussed. The motion of the flight simulation model was restricted to the heave axis, and augmented to include an elastic mode of vibration in addition to the rigid heave degree of freedom. Four different pilots flew several alternative model configurations with different elastic mode frequency and different collective pitch gearing ratios. This resulted in several observable unstable pilot-vehicle interactions at frequencies that cannot be traced back to the rotorcraft dynamics. Unstable oscillatory events evolving into limit cycle oscillations occurred most often at frequencies related to the biomechanics of the flight simulator occupant. They appeared to be task dependent and, in some cases, the trigger could be attributed to specific events. Additionally, it was found that the presence of collective friction alleviates but does not completely eliminate the unstable interactions between the pilot and the rotorcraft. Although not statistically meaningful because of the small set of human subjects available for the study, the results confirmed that the biomechanics transfer function of the pilot is the most influential aspect of the pilot-vehicle system that gives rise to the adverse vertical bounce phenomenon. Additionally, this study gave useful insight into the vehicle parameters that can adversely influence the involuntary interaction of pilots with rotorcraft.

Key words: Pilot-Augmented Oscillations, Rotorcraft-Pilot Couplings, Aeroelasticity, Flight Simulation

1 Introduction

Adverse Aircraft-Pilot Couplings (APCs), and their rotary wing counterpart Rotorcraft-Pilot Couplings (RPCs), have been defined as "unintentional (inadvertent) sustained or uncontrollable vehicle oscillations characterised by a mismatch between the pilot's mental model of the vehicle dynamics and the actual vehicle dynamics. The result is that the pilot's control input is out-of-phase with the response of the vehicle, possibly causing a diverging motion." This definition was proposed by the ARISTOTEL consortium [1] [1–3], a project sponsored by the European Commission within the 7th Framework Programme to deliver tools and techniques for the detection and alleviation of aircraft and rotorcraft pilot couplings.

Aeroelastic effects may become important to this class of phenomena when the dynamics of the vehicle are characterised by low-frequency elastic modes associated with the rotor and the airframe, possibly augmented by a high authority Flight Control System (FCS). In these cases, interaction between the pilot and the vehicle is characterised by involuntary behaviour [4]; i.e. the pilot behaves like a passive filtering element between the vibrating cockpit and the control inceptors. Several events of this nature have been experienced in flight by rotorcraft, as documented in the open literature. Prouty and Yackle [5] report RPC as a possible cause of an accident that occurred to the AH-56 Cheyenne during its troubled development. Parham et al. [6] report APC & RPC problems during the development of the V-22 Osprey. Walden [7] discusses RPC problems associated with the development and operation of several US Navy rotary wing aircraft: the CH-46D and E, SH-60B, CH-53E, V-22A and B, and AH-1Z suffered, at some stage of their development/operation, an adverse aeroelastic interaction with the pilot. A detailed database of RPCs is reported in Appendix A of [1]. This paper focuses specifically on a vehicle-pilot coupling that is peculiar of rotorcraft, called "vertical bounce" or "collective bounce". As shown in the block scheme of Fig. 1, in some conditions the vibratory loads generated by the rotor in the cockpit can cause vertical accelerations of the seat that are transmitted through the pilot's arm to the rotor collective lever. This control chain transmits an oscillating signal to the swashplate, and thus back to the rotor, which is manifest as an additional variation of the rotor blade collective pitch that may cause further vibratory loads. This phenomenon is a serious issue for rotorcraft and is known as the root cause of several rotorcraft accidents (see [1, 7, 8]). As shown by the analyses of [8–10], by coupling the

* Corresponding author.
Email addresses: pierangelo.masarati@polimi.it (Pierangelo Masarati), giuseppe.quaranta@polimi.it (Giuseppe Quaranta), linghai.lu@liverpool.ac.uk (Linghai Lu), mjump1@liverpool.ac.uk (Michael Jump).

[1] http://www.aristotel.progressima.eu/

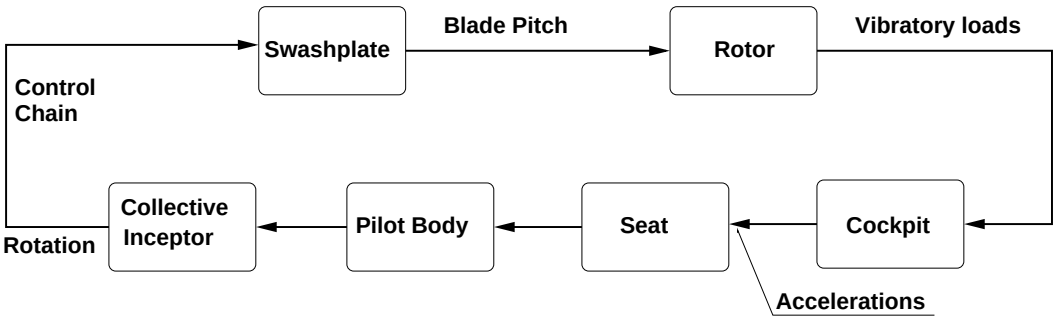

Fig. 1. Block scheme of the vertical bounce feedback loop between the pilot biomechanics and the rotor dynamics.

rotor collective pitching and coning modes with vertical vibratory models of the fuselage and the biomechanical response of the pilots, the study of this phenomenon lies within the discipline of aeroelasticity. As a consequence, the frequency bandwidth to be taken into account is broader than the one usually considered for Pilot Induced Oscillations (PIOs) or classical fixed-wing APCs (conventionally set to 1 Hz in Table 1 of [4], but with the possibility of this being extended to 2 Hz, to be conservative). For example, some of the accidents reported in [7] can be classified as collective bounce with characteristic frequencies up to 6.5 Hz.

Adverse vehicle-pilot couplings have been extensively investigated in relation to voluntary pilot behaviour, especially for fixed-wing aircraft; consider for example the pioneering work done by McRuer et al. (e.g. in [11]). Conversely, the literature is somewhat sparse with respect to involuntary pilot behaviour, the so-called Pilot-Augmented Oscillations (PAO), especially in relation to rotorcraft operations. Several studies have investigated the effects of fixed wing aircraft cockpit manipulators while performing compensatory tracking tasks (for example Magdaleno & McRuer [12] and McRuer & Magdaleno [13]). Subsequent works addressed the impact of vibration on pilot control, focusing on the feedthrough of vibration from the pilot to the control inceptors (for example Allen et al. [14], and Jex & Magdaleno [15]; see also the review by McLeod & Griffin [16] and the work by Merhav & Idan [17]). The effects of lateral stick characteristics on pilot dynamics were further investigated from flight data by Mitchell et al. [18]. However, the collective bounce is a phenomenon peculiar to rotorcraft, since it is related to an interaction with the collective lever, an inceptor typically present only in rotorcraft cockpits (see Figure 2), usually on the left-hand side of the pilot seat. It is used to control the collective pitch of the rotor, i.e. the rotor thrust. Such a control inceptor layout makes it very difficult to use models developed for fixed wing pilots in the context of rotorcraft.

Few works have investigated rotorcraft cockpit layouts. Among them, those of Mayo [20], Parham et al. [6], and Masarati et al. [21], deserve a mention. However, the available literature mainly discusses the characterisation of the

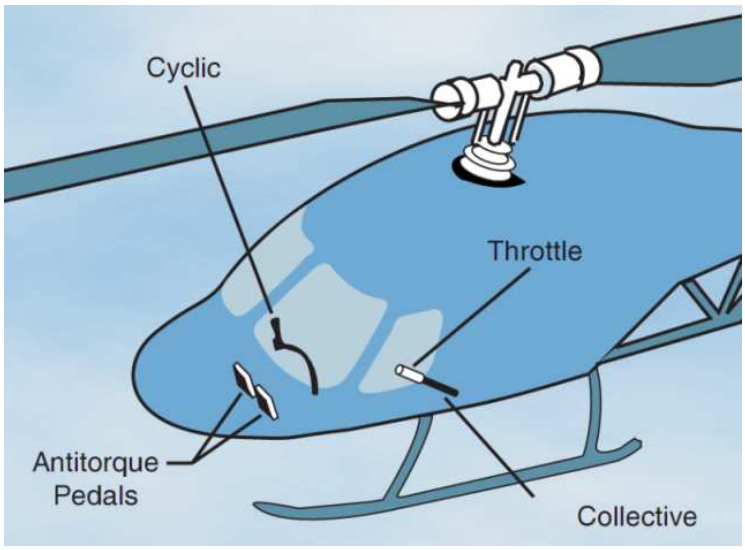

Fig. 2. Layout of typical helicopter cockpit flight control inceptors, from [19]. The collective lever is shown on the left of the pilot seat.

pilot either in-flight (e.g. Refs. [6, 22]) or using flight simulator measurements (e.g. Refs. [20, 21, 23, 24]). In the latter cases, the flight simulator was used as a shaking device to provide excitation to a pilot seated in a realistic cockpit environment. None of the previously mentioned ground-based tests had the pilot in a closed control loop task, and no actual instability resulting from interaction with the rotorcraft was intentionally induced in any of those investigations.

To better study the role of the biomechanical pilot response in the vertical bounce phenomena, a simple experiment that included the use of a flight simulator was jointly designed and conducted by a team of researchers from the University of Liverpool and Politecnico di Milano at the Flight Science and Technology (FST) research facility of the University of Liverpool [25], within the project ARISTOTEL. The experiment aimed to produce unstable events representative of aeroelastic RPCs, or PAOs, under controlled conditions. The purpose was to understand how the involuntary behaviour of the human operator is influenced by participation in an actual Limit Cycle Oscillation (LCO) and the sensitivity of this behaviour to various model parameters. This research was carried out in accordance with The Code of Ethics of the World Medical Association (Declaration of Helsinki) for experiments involving humans.

A highly simplified flight physics rotorcraft model was augmented with an elastic degree of freedom to represent an aeroelastic mode of vibration, yielding a two degree of freedom model (2DOF from this point on). Several rotorcraft aeroelastic modes fall in the range of frequencies that characterise pilot biodynamic feedthrough, see [1, 8]. As a consequence, the generic elastic degree of freedom used in this work can be considered representative of any one of

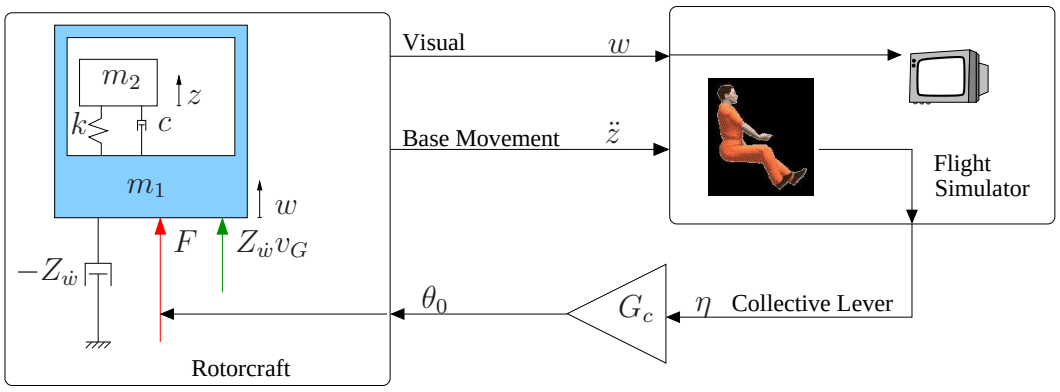

Fig. 3. Block diagram of the aeroelastic RPC simulation test set up.

these modes.

The acceleration of the cockpit that resulted from the dynamic response of the elastic degree of freedom provided the demand to the motion platform of the flight simulator, while the associated visual cues were driven by the overall motion of the vehicle, as sketched in Fig. 3. The motion of the collective control inceptor produced by the pilot, possibly unintentionally amplified as a consequence of the cockpit vibrations, was fed back into the aircraft model to determine the rotor thrust. The control loop closure caused by the pilot introduced the potential for what has been termed a 'bioaeroservoelastic' instability. A parameter called G_c was used to set the gearing ratio between the rotation of the collective lever η and the corresponding rotor collective pitch change θ_0. Additionally, the opportunity to consider a time delay in this control transmission line between the collective lever and the rotor thrust was taken into account. This made it possible to consider the time lag that is intrinsically present in rotorcraft controls due to the thrust generation mechanism (see [26]) but also for the one that can be caused by a fly-by-wire system.

The parameter G_c was used to set the gearing ratio between the rotation of the collective lever η and the corresponding rotor collective pitch change θ_0. Additionally, a variable time delay element was included in the control chain between the collective lever and the rotor thrust. This made it possible to consider the time lag that is not only intrinsically present in rotorcraft control due to the thrust generation mechanism (see [26]) but also for that caused by electronic fly-by-wire systems.

The investigation focused on determining the onset of unstable closed loop oscillations by increasing the gearing ratio between the rotation of the collective control inceptor and the simulated rotor thrust by way of the blade collective pitch. Several combinations of frequency and damping of the elastic mode have been considered, exploring the band between 2.5 Hz and 6 Hz that characterizes significant biomechanical modes involving the vertical vibration of the arms. The presence or absence of simulated friction in the collective

control inceptor has been considered as well. The experiment was designed using the simplified rotorcraft model and Mayo's involuntary pilot model [20] to drive the coupled Pilot-Vehicle System (PVS) unstable for realistic system parameters.

The paper proceeds as follows. The simple dynamic model used for the experimental work is presented first in Section 2. The model was coupled to simple active and passive pilot models, taken from the literature, and analysed to determine the structural properties of the elastic degree of freedom that maximised the chance of driving the coupled pilot-vehicle system into an unstable state during the tests. Section 3 describes the experimental set-up and the test execution. The analysis of the simple model is repeated and discussed for all of the configurations considered in the tests. The results of the tests are discussed in detail in Section 4. The paper finishes with Conclusions drawn from the work.

2 Simplified Aeroelastic Model

This Section describes the simplified model used to prepare the experiment and analyse the results. It consists of the 2DOF model illustrated in the block diagram of Fig. 3. In order to tune the structural parameters of the model, simple mathematical models of the collective control stick motion have been considered. These models account for both the control intentionally introduced by the pilot to perform a tracking task and the one unintentionally fed through the pilot's body and arm as a consequence of the cockpit vibrations. The focus of the experiment and the subsequent analysis is on the unintentional control motions.

2.1 Vehicle Model

The simplified rotorcraft model that was used in the experiment, restricted to motion in the heave axis only, is sketched in Fig. 3. The rigid-body heave equation

$$m_t \ddot{w} = Z \tag{1}$$

describes a perturbation of the equilibrium from the hover; w is the absolute vertical displacement of the vehicle's centre of mass (CM). The vertical force perturbation Z, namely the rotor thrust T minus the weight $m_t g$, is approximated as $Z = Z_{\dot{w}}(\dot{w} - v_G) + Z_{\theta_0}\theta_0$, where v_G is a vertical gust, which plays the role of an external disturbance, and θ_0 is the rotor collective pitch control.

The rigid-body problem is transformed into an aeroelastic one by 'hanging' a second mass onto the rotorcraft, using a spring with stiffness k and a dashpot with damping c. The added mass can be interpreted as the cockpit which adds an inner aeroelastic degree of freedom to the rotorcraft model. The resulting model is defined by Eqs. (2):

$$m_t\ddot{w} - Z_{\dot{w}}\dot{w} = Z_{\theta_0}\theta_0 - Z_{\dot{w}}v_G \tag{2a}$$

$$m_2\ddot{z} + c\,(\dot{z} - \dot{w}) + k\,(z - w) = 0, \tag{2b}$$

with $m_1 = m_t - m_2$ ($m_1 \ll m_2 < m_t$); z is the absolute vertical displacement of the CM of the internal mass m_2, assumed coincident with that of m_t. In the Laplace domain, Eqs. (2) then become

$$w = \frac{1}{s\,(sm_t - Z_{\dot{w}})}\,(Z_{\theta_0}\theta_0 - Z_{\dot{w}}v_G) = H_{w\theta_0}\theta_0 + H_{wv_G}v_G \tag{3a}$$

$$z = \frac{sc + k}{(s^2m_2 + sc + k)}\frac{1}{s\,(sm_t - Z_{\dot{w}})}\,(Z_{\theta_0}\theta_0 - Z_{\dot{w}}v_G) = H_{z\theta_0}\theta_0 + H_{zv_G}v_G. \tag{3b}$$

2.2 Active Pilot Modelling

McRuer's 'crossover' model (see for example [11]) was used to design a pilot model capable of regulating the altitude of the aircraft by producing an adequate voluntary collective control input. The voluntary intervention of the pilot was modelled at this stage to verify that it did not interact adversely with the elastic degree of freedom. The input was the rotorcraft altitude from some desired value, $e = w_d - w$, and the output was the required collective control, θ_0. The product of the pilot model $H_{\theta_0 e}(\mathrm{j}\omega)$ and the error $e = w_d - H_{w\theta_0}\theta_0$ in open-loop can be represented by the transfer function $\mathrm{e}^{-\mathrm{j}\omega\tau_e}\omega_c/\mathrm{j}\omega$, where ω_c is the crossover frequency, specific for a given task, while τ_e is the pilot's time delay. As a matter of fact, according to this model the loop transfer function of a vehicle controlled by a trained pilot does not depend, to some extent, on the characteristics of the piloted vehicle. The desired active pilot model is obtained by considering the rigid vehicle approximation of Eq. (1), which yields an approximate vehicle transfer function

$$H_{w\theta_0}(\mathrm{j}\omega) = \frac{Z_{\theta_0}}{\mathrm{j}\omega\,(\mathrm{j}\omega m_t - Z_{\dot{w}})}, \tag{4}$$

under the assumption that the approximate frequency of the elastic mode, $\sqrt{k/m_2}$, is significantly higher than the crossover frequency. A crossover frequency of 2.0 radian/s and an equivalent time delay of 0.35 s, in accordance with [11], were used in the analysis. A relatively low crossover frequency was used in the subsequent offline analysis because no specific aggression or precision in the execution of the task was requested of the pilots.

2.3 Passive Pilot Modelling

Mayo's passive pilot model [20] yields $\ddot{z}_h$, the absolute vertical acceleration of the hand that grasps the collective control inceptor as a function of the cockpit's vertical acceleration, $\ddot{z}$. It models the biodynamic feedthrough of the pilot, namely the involuntary control produced by the pilot as a consequence of the acceleration of the cockpit. Two functions are proposed for 'ectomorphic' (for individuals with a small and lean build) and 'mesomorphic' (for individuals with a large bone structure and muscle build) test subjects. These models were obtained from only a few tests conducted using a small number of subjects and with just one cockpit layout. Several other tests have highlighted that the pilot biodynamic response may significantly depend upon the mechanical characteristics and layout of the inceptors, and also on the pilot's task [27, 28]. Numerical investigation conducted on detailed models of the pilots' arm muscles showed that the numerical transfer function can be modified in a non-trivial manner by changing the activation of the muscles in such a way that the global equilibrium is not affected [29]. As a consequence, Mayo's models may only be considered roughly representative of a pilot's biomechanical behaviour and not a universally valid model. A better approach to model the involuntary behaviour of the pilot for rotorcraft design considers the pilot as an uncertain element, as proposed in [30, 31], exploiting the robust analysis approach. However, since, in the present case, the pilot involuntary model was merely used to estimate the order of magnitude of the parameters to be used in the subsequent experiment, the adoption of a simple model such as Mayo's was considered acceptable.

The rotation of the collective control inceptor can be estimated by subtracting the absolute acceleration of the seat from the absolute acceleration of the hand to obtain the relative acceleration of the hand. Integrating this result twice yields the relative displacement of the hand. By dividing such displacement by the length of the collective control inceptor, L_ψ, and the end-to-end rotation of the device, $\Delta\psi$, the normalised rotation of the inceptor, η, as a function of the cockpit acceleration can be obtained,

$$H_{\eta\ddot{z}}(s) = \frac{H_{\ddot{z}_h\ddot{z}}(s) - 1}{s^2 L_\psi \Delta\psi}. \tag{5}$$

In the case of Mayo's functions, $H_{\eta\ddot{z}}(s)$ becomes

$$H_{\eta\ddot{z}}(s) = -\frac{1}{sL_\psi\Delta\psi}\frac{s + 1/\tau_p}{s^2 + 2\xi_p\omega_p s + \omega_p^2}, \tag{6}$$

using the data from Table 1. The involuntary pilot model of Eq. (6), with data for the ectomorphic pilot, is used in this work. The other parameters have been estimated from the University of Liverpool's HELIFLIGHT system [25]

Table 1
Data for function $H_{\eta\ddot{z}}(s)$ from Mayo's models.

	ectomorphic	**mesomorphic**
ω_p (radian/s)	21.267	23.567
ξ_p	0.322	0.282
τ_p (s)	0.118	0.108

as $L_\psi = 0.35$ m, $\Delta\psi = 45$ deg. The rotation of the inceptor normalised with respect to its end-to-end rotation is transformed into the actual rotor blade collective pitch demand by means of a gearing ratio G_c, whose reference value has been set to 20 deg (about 0.35 radian), i.e. the end-to-end rotor blade collective pitch angle. The double integration ($1/s^2$ in Eq. (5)) has been multiplied by a second-order Butterworth high-pass filter, to avoid interference with the active pilot model's behaviour, resulting in

$$H_{\eta\ddot{z}}(s) = -\frac{1}{L_\psi \Delta\psi} \frac{s + 1/\tau_p}{s^2 + 2\xi_p\omega_p s + \omega_p^2} \frac{s}{s^2 + \sqrt{2}\omega_h s + \omega_h^2}. \tag{7}$$

with $\omega_h = 10$ radian/s (5 times ω_c). The positive (lead) phase shift introduced by such a filter is comparable to that introduced by the wash-out filters of the flight simulator during the experiment.

The results of the experiment, discussed later, suggest that the pilot feedthrough model proposed by Mayo may be overly conservative, since instabilities were only found for gearing ratios larger than predicted, often more than twice as large.

2.4 Loop Transfer Function

The feedback loop is closed by writing the collective pitch angle, θ_0, as the combination of the contributions produced by the active and passive pilot models, namely

$$\theta_0 = H_{\theta_0 e}\,(w_d - H_{w\theta_0}\theta_0) + G_c H_{\eta\ddot{z}} s^2 H_{z\theta_0}\theta_0. \tag{8}$$

The corresponding loop transfer function,

$$H_L = H_{\theta_0 e} H_{w\theta_0} - s^2 G_c H_{\eta\ddot{z}} H_{z\theta_0} = \mathrm{e}^{-\mathrm{j}\omega\tau_e}\omega_c/\mathrm{j}\omega - s^2 G_c H_{\eta\ddot{z}} H_{z\theta_0}, \tag{9}$$

expresses the important fact that the element related to the voluntary behaviour of the pilot is not explicitly affected by the value of the gearing ratio, G_c, nor by any time delay in the control chain. In fact, a trained pilot quickly adapts to (limited) changes in such a gain parameter, by updating his or her

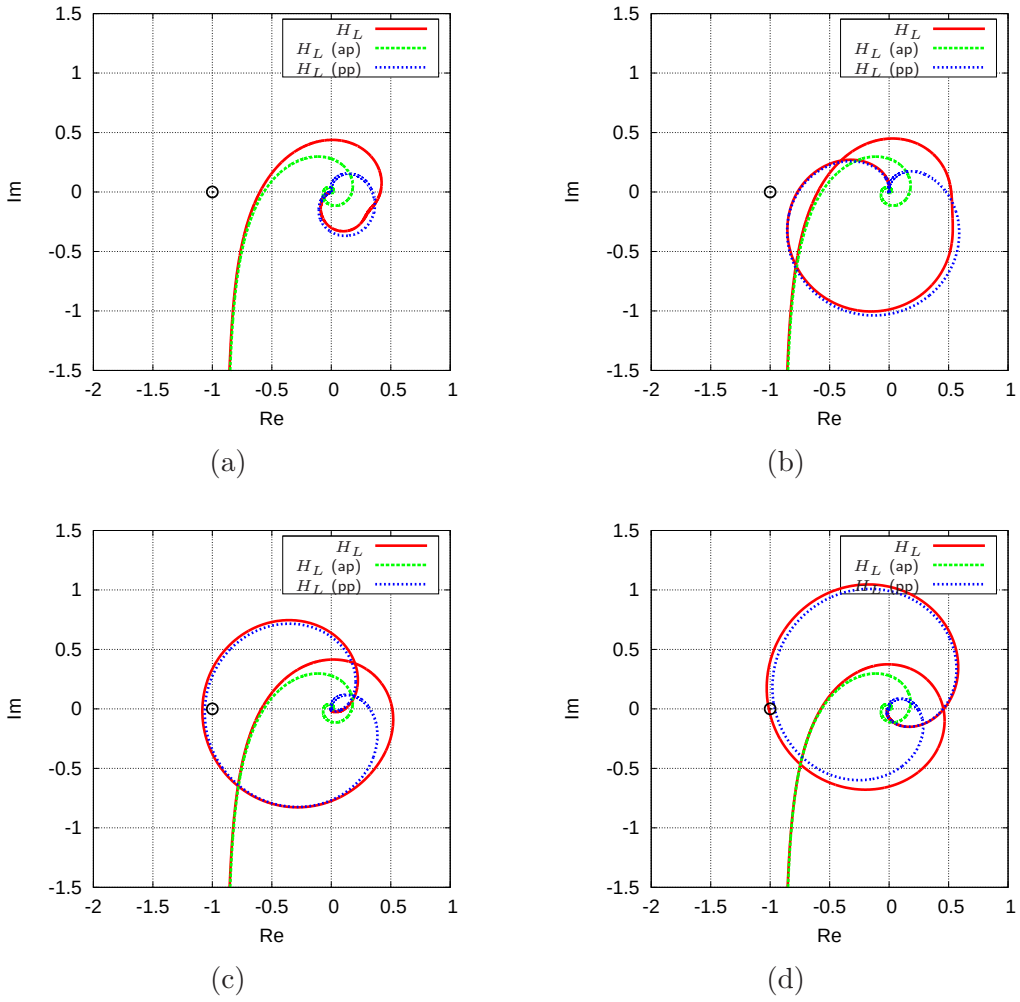

Fig. 4. Nyquist plot of loop transfer function (H_L), split into active ($H_{\theta_0 e} H_{w\theta_0}$, 'ap') and passive ($-s^2 G_c H_{\eta \ddot{z}} H_{z\theta_0}$, 'pp') pilot contributions; (a): no elastic mode; (b) with elastic mode at about 3.5 Hz; (c) with elastic mode at about 3.5 Hz and 50 ms time delay; (d) with elastic mode at about 3.5 Hz and 100 ms time delay.

mental model of the vehicle dynamics being controlled and thus compensates for such changes. On the contrary, the element related to the involuntary behaviour is (linearly) affected by the gearing ratio. For this reason, that parameter was selected as the main driver to influence the behaviour of the coupled pilot-vehicle system during the experiments.

Figure 4 shows the Nyquist diagram of the loop transfer function of Eq. (9) using the structural and aerodynamic properties of a helicopter of the class of the Sud Aviation SA330 Puma. In this model m_2, c, k, and G_c were tuned, within realistic limits, to yield an instability for an elastic mode slightly above 3 Hz. This frequency is in the vicinity of the first biomechanical mode of the pilot holding the collective control inceptor, according to Mayo's' functions of Table 1 [20] and other experimental evidence [21]. The active pilot contribution

Fig. 5. University of Liverpool's HELIFLIGHT Flight Simulator.

is essentially unchanged by the elastic mode; the destabilising contribution of the passive pilot model is clear when the elastic mode is present. The degree of system stability can be inferred from the Nyquist plot by evaluating the distance of the loop frequency response functions from the point $(-1 + \mathrm{j}0)$. If the plotted curves encircle the point $+(-1 + \mathrm{j}0)$ clockwise, the closed loop system becomes unstable (see [32], pp. 155–156). From the plots in Figs. 4(b–d), one can infer that a time delay between the motion of the control inceptor and the force, for example caused by a flight control system, may increase the proneness of the pilot-vehicle system to instability by rotating the lobe of the plot clockwise.

3 Experimental Activity

3.1 Experiment Description

The aircraft model of Eqs. (2) was realised in state space form in the FLIGHTLAB software environment incorporating the data from Table 2. The real-time simulation output of this model were then used to drive the motion platform control system and external world visualisation. Global data related to the SA330 Puma were obtained from Ref. [26]. Modifications to most of the model parameters required that the flight simulator be stopped and the model reloaded. Modification to the gearing ratio G_c was performed 'on the fly' and was used as a means of changing the behaviour of the system and to try to induce an instability during the tests. The frequency and amplitude of the disturbance force was also varied to increase the difficulty of the piloting task in an attempt to trigger a PAO event.

Table 2
Nominal model data.

m_t	(kg)	5805.0
$Z_{\dot{w}}$	(N·s/m)	-0.320·m_t
Z_{θ_0}	(N/radian)	85.0·m_t
m_2	(kg)	70.579
c	(N·s/m)	631.11
k	(N/m)	35203.0
τ_e	(s)	0.35
ω_c	(radian/s)	2.0
L_ψ	(m)	0.35
$\Delta\psi$	(radian)	0.79
G_c	(radian)	0.35

The test campaign was conducted in July 2011 at the University of Liverpool using the HELIFLIGHT flight simulator (Fig. 5), involving three engineer (i.e. non-professional) pilot subjects (pilots 1, 2, and 3) and one professional (currently a fixed-wing airline, but formerly a helicopter test) pilot subject (pilot 4). Clearly, the limited number of subjects involved in the test, determined by cost and availability of the flight simulator, affects the statistical relevance of the results; as a consequence, the results of the experiment should be considered exploratory rather than conclusive.

Only the interaction of the pilot with the collective control inceptor was considered in the test. All of the other inceptors in the cockpit were inactive, i.e. their use did not affect the states of the simulation model. The relevant properties of the inceptor are indicated in Table 2. The motion of the inceptor is controlled by an electric motor whose torque can be set to reproduce a prescribed amount of friction. In most cases, minimal torque (ideally, zero) was demanded in the test set-up, unless otherwise specified. As a consequence, the control inceptor was expected to only provide inertial reaction to motion caused by the pilot's feedthrough. Since this set-up is consistent with that used in the feedthrough characterisation experiments performed by Mayo [20], and thus inertial reaction is already accounted for in the feedthrough function, stick characteristics have not been explicitly considered in the analysis.

The test matrix consisted of a configuration without the elastic mode, which simulations predicted to be free from unstable RPCs, and several permutations of the previously mentioned reference configuration with the elastic mode tuned for marginal stability, obtained by changing the stiffness k and the damping c as indicated in Table 3. During each test, different levels of gearing

ratio G_c and of external disturbances (frequency, ranging from 0.25 Hz to 1 Hz, and amplitude, ranging from zero to 'noticeable' by the pilot but never to a magnitude that interfered with the flight task) in the form of gust velocities have been considered. Further investigation involved changes to the task (from position hold to position capture and hold) and to the level of friction in the collective control inceptor.

The simulator's motion base unit receives its translational motion demands in terms of specific force (acceleration, in m/s^2) from the simulation flight physics model. The motion drive algorithms transform these demands into hexapod leg length to drive the electric motors. The base unit's filter system comprises a set of saturation, washout and low-pass filters. The saturation function limits acceleration demands to a user-defined value, 2 m/s^2 for this experimental set-up; the transfer function of the high-pass washout filter used for the experiment was $H_A(s) = s/(s+3)$, while that of the low-pass filter that double-integrates the specific force demand was $H_B(s) = 1/(s+3)^2$. The three poles are thus coincident.

Measurements consisted of relevant outputs from the flight simulator, namely the motion demands and responses of the platform actuators, the vehicle states and the positions of the control inceptors. In addition, the translational accelerations and rotational rates of the motion-base itself were measured using a MicroStrain 3DM-GX1 motion sensor (triaxial accelerometer and gyro). Of course, only a heave acceleration would be measured for the experiment described herein. The measured accelerations of the flight simulator matched reasonably well those measured at the pilot's seat in the frequency band of interest for the test (1 Hz to 10 Hz). Indeed, the seat is actually an integral part of the motion base structure. The pilot arm motion was measured by three Xsens MTi motion sensors (triaxial accelerometers and gyros) strapped both to the left arm as close as possible to the subject's wrist and elbow, and to the left shoulder. An analogous experimental set-up used in previous tests is described in detail in [21]. The correspondence of seat and motion base accelerations was empirically checked by clamping a MTi sensor to the simulator seat and then comparing the spectrum of the measured acceleration with that of the acceleration measured at the motion base.

3.2 Pilot Task Description

Each pilot was asked to perform a task based upon the vertical manoeuvre specified in the United States rotorcraft handling qualities performance design specification, ADS-33E-PRF [33]. The pilot's view of the task course, as configured in the HELIFLIGHT simulation facility, is shown in Fig. 6. The course consisted of a vertical column, marked at 25 ft (about 7.6 m) intervals with

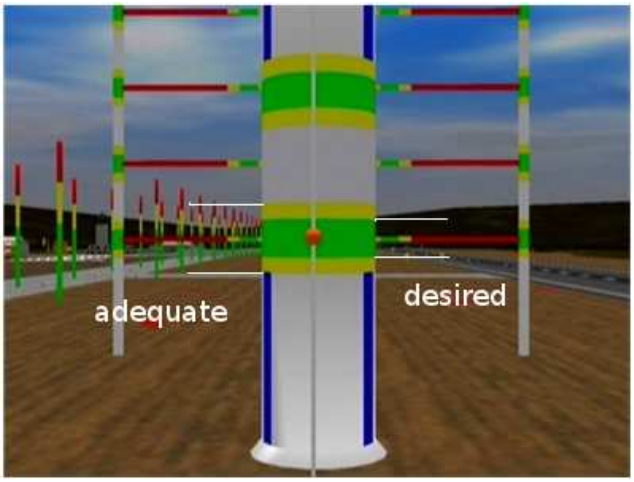

Fig. 6. Illustration of the task for 2DOF PAO testing.

green (inner, labelled as 'desired') and yellow (outer, labelled as 'adequate') bands. Each band provided the pilot with a visual cue of the desired and adequate hover task performance standards, ±1.5 ft (0.46 m) and ±3 ft (0.91 m) respectively. The pilot was able to judge his or her performance against this standard using the thin pole and ball feature located in front of the vertical column. The pilot's task was therefore to keep the rotorcraft model at an approximately constant altitude, using only the collective lever, by locating the ball within the bands indicated on the column whilst the model was subjected to the various experimental disturbances. When instructed by the test director, the pilot's secondary task was to depart from the hover and either climb or descend through 50 ft (about 15 m) and re-stabilise into a hover at the appropriate column band location. When climbing, the secondary task was more demanding than in descent, especially for taller pilots, because of the limited upwards view available in the simulator. This caused a more 'sudden' appearance of the bands in the pilot's field of view, when ascending, requiring a more aggressive control input to capture the desired altitude. As previously shown in Fig. 3, the outside world visual display was driven by the 'rigid body' motion of the rotorcraft model whilst the motion cues were driven by a combination of the rigid body and aeroelastic degrees of freedom.

3.3 Tested Configurations

Figure 7 shows the Nyquist plots of the loop transfer functions that were tested during the campaign. Only the configurations nominally without collective control friction presented in Table 3 are shown in the plots. The configurations with nominal friction are not considered because a (quasi-)linear model would not be representative of the actual behaviour. As shown in Table 3, the configurations tested with friction usually had very low structural damping

Table 3
Tested configurations.

Case #	Pilot	k/k_{ref}	c/c_{ref}	friction	freq. Hz	damp. %
1	2	0.50	0.15	on	2.53	4.29
2	1,2,3,4	0.50	0.40	off	2.51	11.41
3	2	1.00	0.10	on	3.58	2.02
4	1	1.00	0.20	on	3.57	4.04
5	1,2,3,4	1.00	1.00	off,on	3.50	20.15
6	1,2	1.60	0.40	off	4.51	6.38
7	2,3	1.60	0.70	off	4.50	11.15
8	1,2	1.60	1.00	off	4.47	15.93
9	2	2.80	0.35	off	5.98	4.22
10	1,2,3	2.80	0.50	off	5.97	6.02
11	1	2.80	1.00	off	5.94	12.04
12	1,2,3	3.00	3.00	off,on	5.80	34.89

associated with the elastic mode, in an attempt to induce PAO despite the nonlinearity in the control inceptor.

The stability of the coupled system predicted by this simple analysis was only partially confirmed by the tests. It is worth recalling that the model is "exact", in the sense that the numerical model of the system was actually the driver for the flight simulator's motion base. The uncertain part of the system shown in the plots of Fig. 7 is related to the pilot's behaviour.

Case #5 consists of the nominal stiffness and damping coefficients, which yield an elastic degree of freedom frequency of about 3.55 Hz with 20% damping. Figure 7(a) clearly shows that it was designed to yield a marginally stable system when interacting with the passive pilot model.

Case #12 consists of very large stiffness and damping coefficients, to push the elastic mode above the characteristic frequency of the passive pilot to prevent their interaction.

The other cases were obtained by reducing and increasing the stiffness and the damping of the elastic degree of freedom, in an attempt to highlight the stability properties of the coupled pilot-vehicle system.

Some of the test cases, for example Case #6, were designed following the

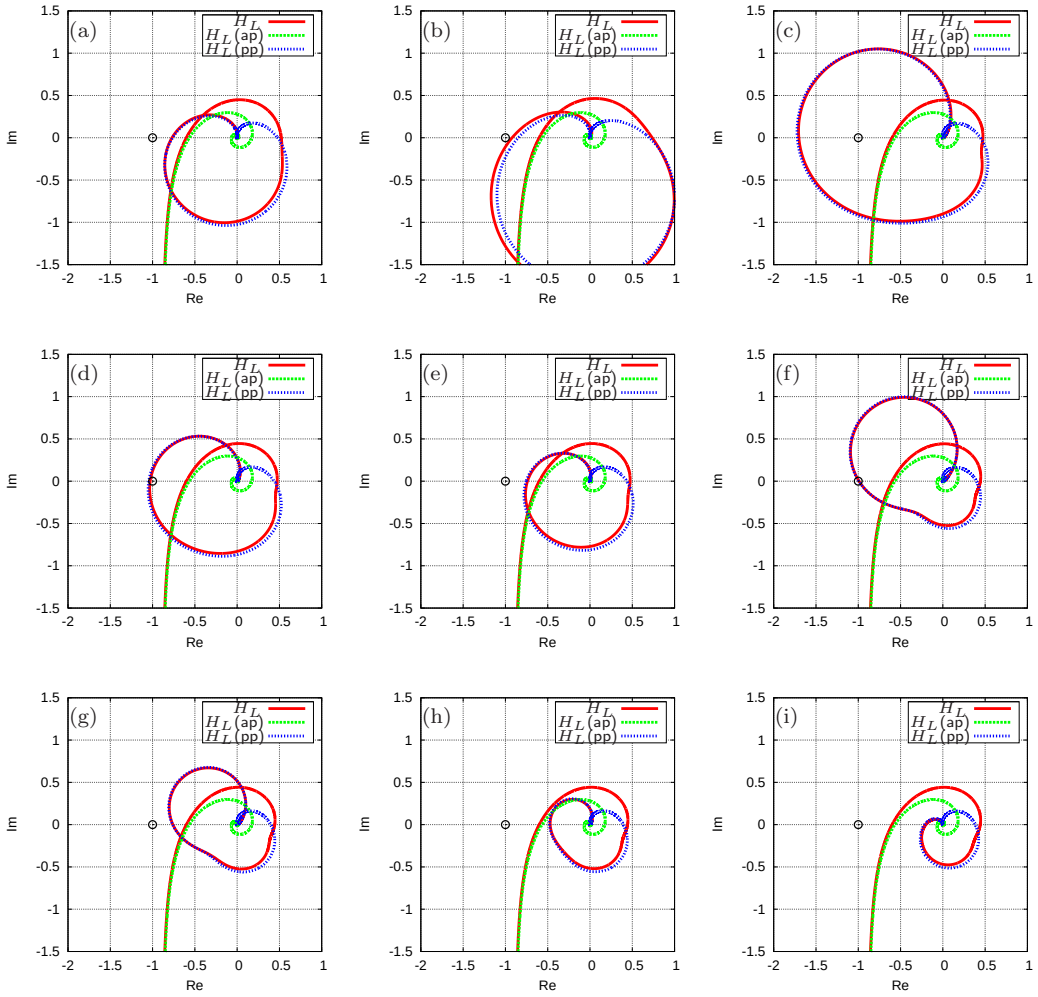

Fig. 7. Nyquist diagrams of the configurations tested without friction, with the nominal gearing ratio G_c. The separate contribution of the active (ap) and passive (pp) pilot models is depicted; (a): case #5; (b): case #2; (c): case #6; (d): case #7; (e): case #8; (f): case #9; (g): case #10; (h): case #11; (i): case #12.

observation that similar cases (#7 and #8, with the same stiffness but with larger damping) did not result in a clear PAO instability. Figure 8 clearly shows the effect of the damping on the stability of the coupled system: for a stiffness $k/k_{\text{ref}} = 1.6$, as the damping c/c_{ref} is reduced from 1.00 to 0.40, the lobe corresponding to the pilot mode grows until an instability is encountered.

Cases #9, #10 and #11 show a similar trend. In this case, the stiffness was set to $k/k_{\text{ref}} = 2.8$, to place the structural mode at about 6 Hz, while the damping c/c_{ref} is reduced from 1.00 to 0.35. The reason for this was to assess the possibility of achieving a system instability involving a higher biomechanical mode highlighted in previous tests [21, 22], but that is not present in Mayo's models. A behaviour similar to the previous cases is observed in Fig. 9.

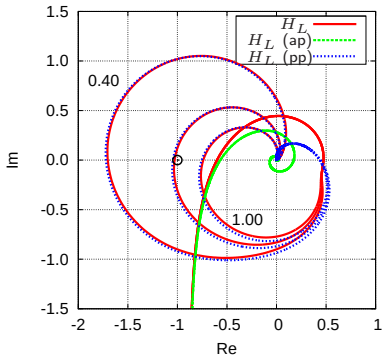

Fig. 8. Nyquist plots of loop transfer functions with $k/k_{\text{ref}} = 1.6$ and $c/c_{\text{ref}} = 0.40$, 0.70, 1.00.

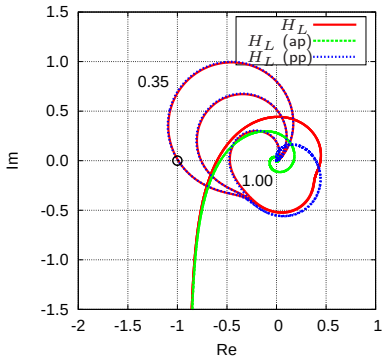

Fig. 9. Nyquist plots of loop transfer functions with $k/k_{\text{ref}} = 2.8$ and $c/c_{\text{ref}} = 0.35$, 0.50, 1.00.

The results shown in Fig. 7 do not include the filters between the requested and the actual motion of the base. Since the filters significantly depart from double integration ($1/s^2$) only at low frequency (about 0.5 Hz), because of the washout term, they have a substantial impact in the band of frequencies of interest for the active pilot model, while they minimally affect the band of interest for the passive pilot. As a consequence, they have not been considered in the analysis. In addition, of course, the saturation of the acceleration cannot be modelled by a simple linear model in the frequency domain. This approximation is believed to be conservative.

4 Discussion of Results

This section discusses in detail the results of the tests. An appreciably large database has been collected, consisting of:

- flight dynamics model output (motion demands);
- flight simulator motion base measurements (actual motion output);

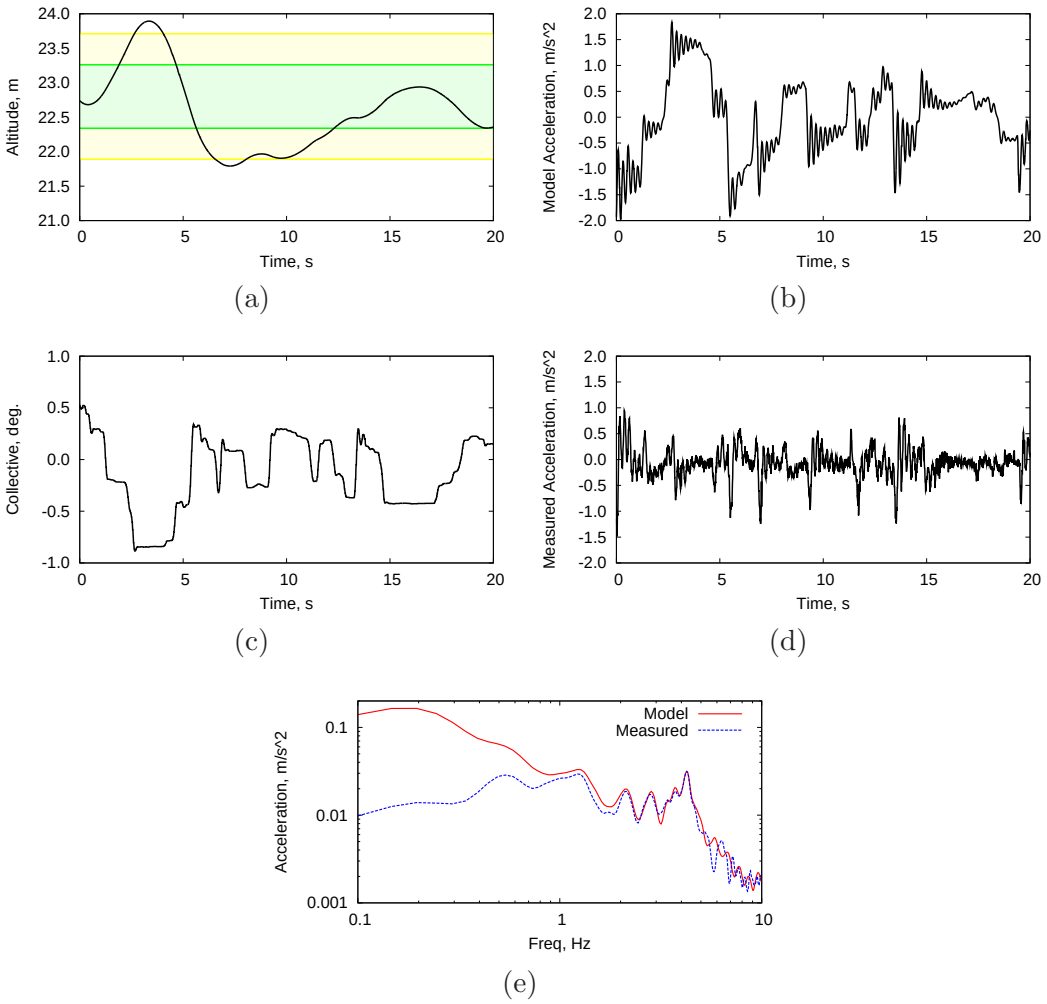

Fig. 10. Test measurements in a marginally stable case; (a): rotorcraft altitude (darker (green) band: desired performance, lighter (yellow) band: adequate performance), (b): model vertical acceleration, (c): collective pitch input, (d): measured vertical acceleration, (e): amplitude of Fourier transform of accelerations.

- cockpit inceptor motion;
- pilot biomechanics measurements;
- pilot comments and ratings, where applicable.

The main results are discussed in the following. A marginally stable and a slightly unstable case are described first, to highlight the mechanics of the closed loop instability. Subsequently, the effects of frequency and damping of the structural mode are discussed. Finally, results with emulated friction in the collective control inceptor are analysed.

4.1 Marginally Stable Case

An example of a typical result obtained with a lightly damped elastic mode is shown in Fig. 10. The model of Case #6 was used with a gearing ratio G_c of 0.80 radian, more than twice the nominal value, and a disturbance signal close to 1 Hz. During this time interval, the pilot was trying to keep the (red) ball inside the adequate limits prescribed for the task (the outer yellow bands on the vertical pole of the test course, Fig. 6), as shown by the time history of the altitude, Fig. 10(a) (desired and adequate performances are indicated in the figure by corresponding darker (green) and lighter (yellow) bands). The pilot's comments associated with this case indicate a high workload was required even to achieve this relatively poor task performance. Figures 10(b) and 10(d) respectively show the vertical acceleration simulated by the numerical model and that measured on the motion base. The low frequency accelerations that appear in the response of the model are filtered by the simulator washout, while the high frequency content of the two signals is quite close. In fact, the FFT diagram of those signals, Fig. 10(e), shows almost coincident peaks between 2 and 5 Hz. Both FFT diagrams clearly show a peak at 4.3 Hz, a frequency close to that of the elastic degree of freedom. The damped oscillation is also visible in the acceleration time history of the model. However, the time history of the collective control inceptor does not show any high frequency content, a clear indication of the absence of RPC. The FFT of the computed vertical acceleration shows significant activity centred about 0.2 Hz, a consequence of the intentional actions the pilot performs to achieve the prescribed task. Therefore, although during this test the pilot perceived a high workload, no noticeable biodynamic couplings occurred. The difference between the requested and the actual acceleration frequency content curves of Fig. 10(e) is a consequence of the washout filters of the flight simulator motion base, which filter motion requests below about 0.5 Hz. Such frequency is well below that of the feedthrough phenomenon of interest (3 Hz to 5 Hz), so the incorrect low frequency motion of the platform should not directly affect the high-frequency involuntary feedthrough. Whether the low-frequency behaviour of the vehicle, which influences the voluntary action of the pilot (e.g. by producing cues), could act as a trigger for the high-frequency involuntary feedthrough remains an open question.

4.2 Slightly Unstable Case

A typical example of a result obtained when the coupled system was driven into a slightly unstable condition is shown in Fig. 11. The model configuration was again that of Case #6, with a gearing ratio G_c of 1.2 radian, more than three times higher than the nominal value. An unstable oscillation clearly starts at

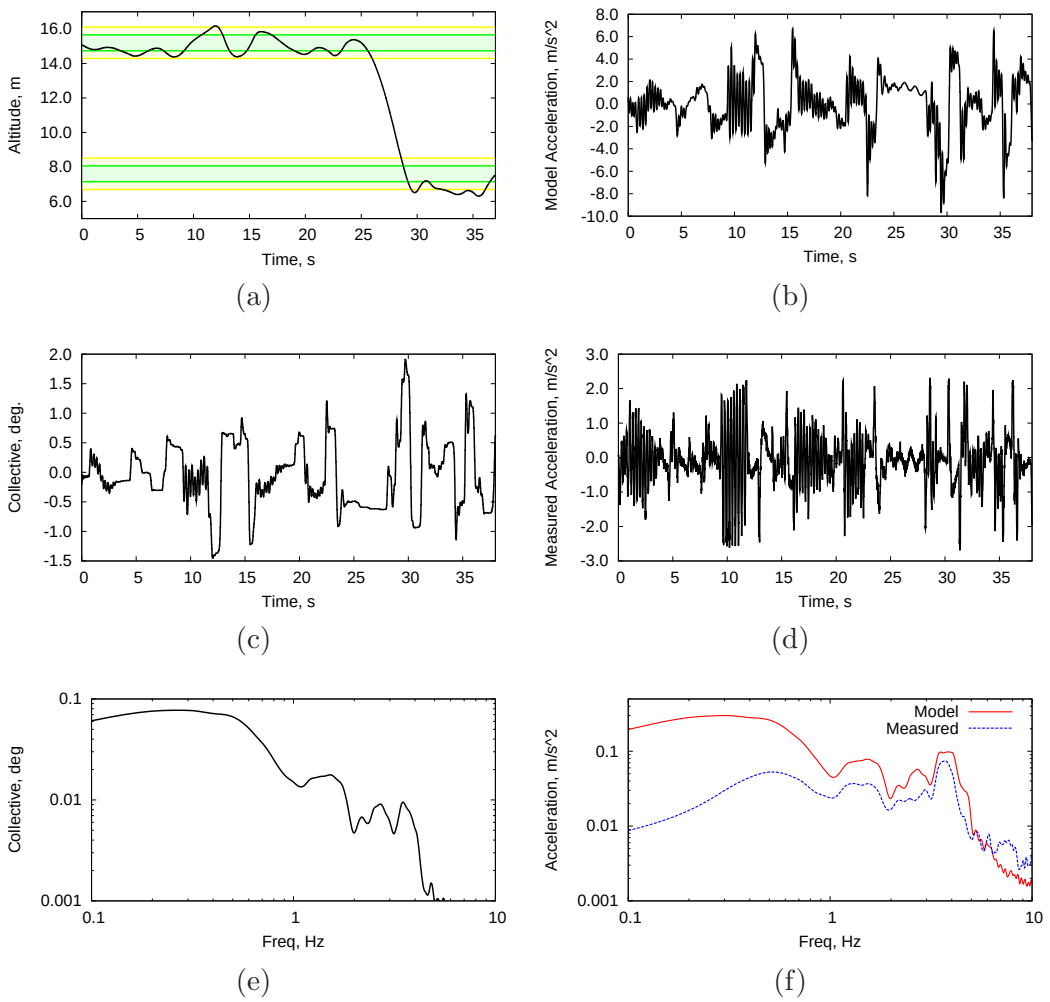

Fig. 11. Test measurements in an unstable case; (a): rotorcraft altitude (darker (green) band: desired performance, lighter (yellow) band: adequate performance), (b): model vertical acceleration, (c): collective pitch input, (d): measured vertical acceleration, (e): amplitude of Fourier transform of collective pitch input, (f): amplitude of Fourier transform of accelerations.

about $t = 10$ s and lasts for about 3 s in the time history of the collective lever, Fig. 11(c), along with several other incipient oscillations. In the same time interval, the vertical acceleration of the model, Fig. 11(b), oscillates at high frequency with an amplitude slightly above the saturation limit of 2 m/s^2, whereas the measured acceleration, Fig. 11(d), clearly reaches the saturation limits. This is an unambiguous unstable RPC event that evolved into a LCO due to the demand saturation limits of the flight simulator motion filters. The LCO condition was clearly perceived and reported by the pilot. Note that during the LCO event the pilot was hardly able to maintain the aircraft within acceptable performance boundaries, as shown in Fig. 11(a).

The FFT of the collective lever motion and of the cockpit accelerations,

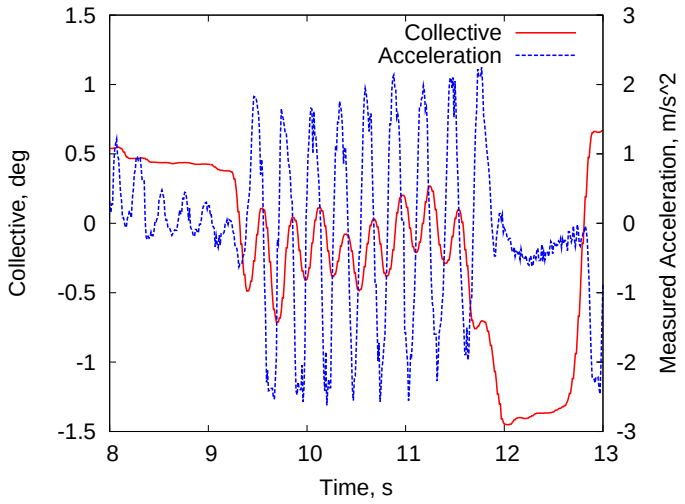

Fig. 12. Close-up of the RPC event of Fig. 11.

Figs. 11(e–f), clearly show a peak at 3.8 Hz. In this case, the noticeable differences in the frequency content of the acceleration curves can be explained by considering the appreciable intervention of the saturation in the motion base demand. Such difference is greatly reduced above 1 Hz, suggesting that the effect of the saturation on the feedthrough phenomenon of interest should not be critical.

The structural mode peak at 4.3 Hz is somewhat visible in the FFT of the accelerations, whereas it is absent in that of the collective lever. Thus, the instability occurs at a frequency that is not present in the numerical model of the aircraft nor in the gust forcing term. As a consequence, the only element in the feedback loop that can introduce this peak is the pilot's biodynamics. A closer look at the RPC event itself, Fig. 12, shows how the collective input and the measured acceleration of the motion base are almost 90 degrees out of phase while these two signals are expected to be 180 degrees out of phase under normal conditions. Consider the equivalent mechanical model of the system shown in Fig. 13, where the biodynamics of the pilot are further approximated as a lumped mass m_p, a spring of stiffness k_p and a dashpot of damping c_p. The phase relationship between the acceleration of the vehicle and the collective control when the instability occurs is illustrated in Fig. 14 and explained in the following. When the system vibrates in the vicinity of the frequency of the elastic mode, the displacements z_1 and z_2 are (almost) in phase opposition (Fig. 14(a)). This is exactly true when no structural damping, c, is present. Each acceleration is naturally in phase opposition with the corresponding displacement (Fig. 14(b)). In fact, neglecting initial conditions, $\mathcal{F}(\ddot{z}) = -\omega^2\mathcal{F}(z)$, where $\mathcal{F}(\cdot)$ denotes the Fourier transform operator. As a consequence, $\ddot{z}_2$ is almost in phase with z_1. The acceleration $\ddot{z}_2$ induces the involuntary collective input, θ_{pp}, which is related to the difference between the absolute motion of the pilot, z_p, and that of the cockpit, z_1. The involuntary

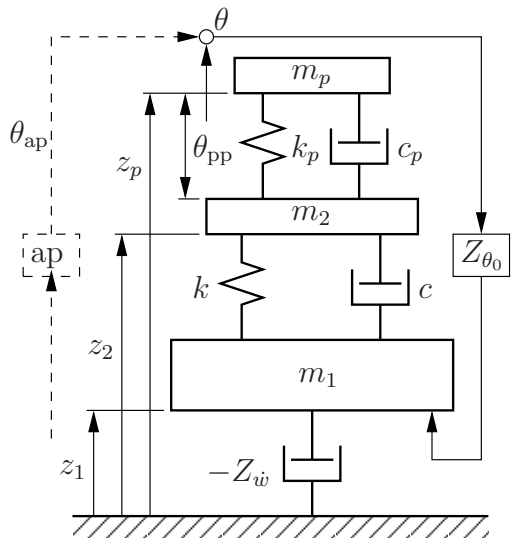

Fig. 13. Equivalent mechanical system of the 2DOF problem including the pilot.

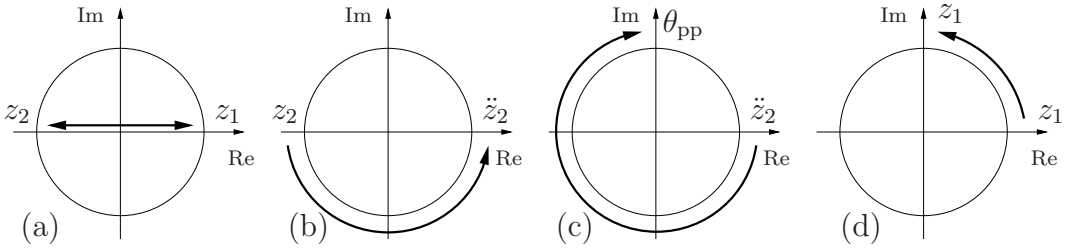

Fig. 14. Phase relationships among variables of the 2DOF problem. The relationship among figures (a)–(d) is described in the text.

collective input, were the involuntary pilot model behaving statically, would be exactly in phase opposition with the input; in fact, an upward acceleration would result in a downward rotation of the collective, and vice versa. However, assuming that the involuntary pilot model can be approximated using a simple mass, a spring and a dashpot as shown in Fig. 13, when the frequency of vibration is also close to the resonance of the pilot model, a further delay of the order of 90 degrees appears in the involuntary collective motion, since z_p, the motion of a damped oscillator at resonance, would lag 90 degrees behind z_2, the forcing term. As a consequence, the collective now lags 270 degrees behind the acceleration $\ddot{z}_2$ (Fig. 14(c)), and thus behind z_1. This implies that the force generated by the involuntary deflection of the collective, $\Delta Z = Z_{\theta_0}\theta_{\mathrm{pp}}$, is exactly in phase with the velocity $\dot{z}_1$ of the point it is applied to, which leads z_1 by 90 degrees (Fig. 14(d)), since $\mathcal{F}(\dot{z}) = \mathrm{j}\omega\mathcal{F}(z)$. Therefore, a positive power is produced that continuously 'pumps' energy into the system for the entire duration of a cycle. When this energy is greater than the energy dissipated by the damper and by the aerodynamics, the instability illustrated in Fig. 12 occurs. To escape from the unstable RPC condition of Fig. 12 the pilot had to apply a significant and abrupt change to the collective position (at about $t = 12$ s).

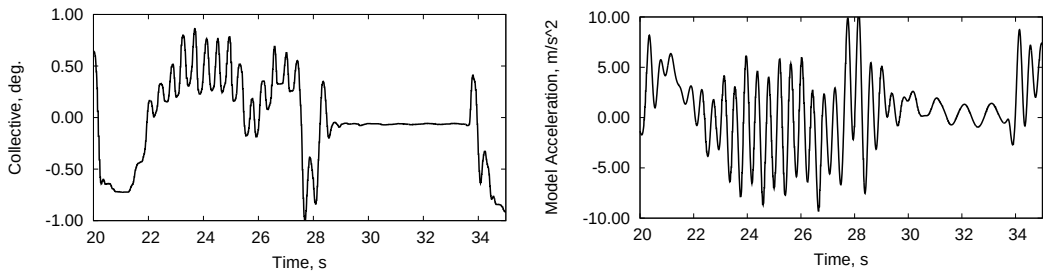

(a) (b)

Fig. 15. The effect of releasing the stick while experiencing an unstable oscillation; (a): collective pitch input, (b): vertical acceleration.

The altitude loss shown in Fig. 11(a) after $t = 25$ s is the consequence of repositioning the vehicle model at a column band 25 ft (7.6 m) lower than the task start position. This manoeuvre brought the unstable RPC to a stop. In fact, the incipient unstable oscillation visible in the acceleration signals between $t = 20$ s and $t = 25$ s is completely cancelled by the action on the collective made by the pilot to reach a target at a lower altitude. In the time frame between $t = 25$ and $t = 27$ s, while the aircraft is changing altitude and the pilot is holding the collective lever almost still, all the high frequency oscillations disappear from the acceleration signals, except for the disturbance signal at about 1 Hz. This is interpreted as the change in task, from a precision task to a manoeuvre, changes the neuromuscular state of the pilot and drives the coupled system away from instability.

Additional evidence for the biodynamic nature of the unstable phenomenon experienced during this test campaign is offered by the data shown in Fig. 15. They refer to a test performed with the configuration of Case #5. In that case, the sustained high frequency oscillations observed between $t = 28$ and 34 s stopped when the control inceptor was released by the pilot, thus opening the feedback loop.

It is worth considering that in most cases a marginally stable behaviour was observed only after the gearing ratio was increased to a value higher than that predicted by the analytical model, usually about twice as large, and in some cases even eight times larger; significant variability was observed among the flight simulator occupants. Both inter-subject variability, i.e. variability among different human subjects, and intra-subject variability [34], i.e. variability of biomechanical behaviour of the same subject in different conditions, were observed. Since the flight dynamics model was simple and exact, and the flight simulator base adequately reproduced the requested motion, the consistent under-prediction of the stability limit must be related to the uncertainty and variability of the biomechanical behaviour of the human component of the system. The results of this test seem to indicate that predictions using the transfer functions proposed in [20] are conservative. Safety was never a con-

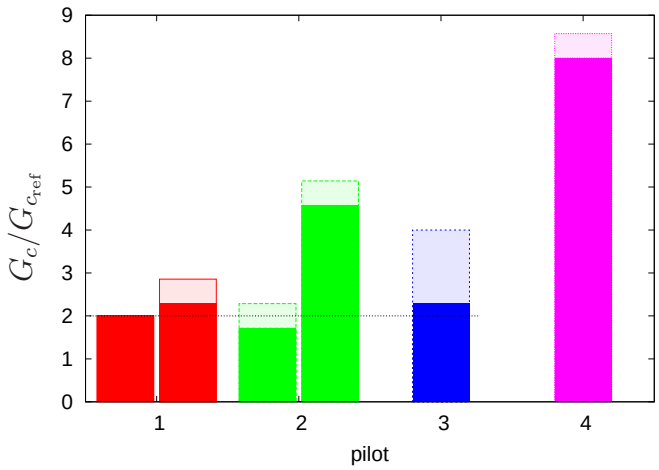

Fig. 16. Gearing ratios $G_c/G_{c_{\mathrm{ref}}}$ tested by all pilots with nominal properties of elastic degree of freedom; shaded: highest tested value; solid: first observed instability.

cern, since changing the control attitude or releasing the control immediately interrupted any unstable behaviour.

4.3 Gearing Ratios with Nominal Elastic Mode Properties

Figure 16 shows the gearing ratios, G_c, experienced by the four pilots in different test sessions using the nominal stiffness and damping values for the elastic degree of freedom. The shaded portion of the bars indicates the largest value tested in the session, while the solid bar indicates the value corresponding to the first observed instability.

Engineer, non-professional but experienced simulator pilots (1–3) showed a PAO instability at about 3.5 Hz for G_c values between 0.6 and 0.8 radian (about twice the reference value), while the professional pilot (4) only encountered it at very large G_c. Measurements related to pilot 4 actually show oscillations at about 2.8 Hz (Table 4); however, they are masked by significant intentional control activity being exerted to perform the prescribed task. The pilot perceived the instability only for $G_c \geq 2.8$ radians, although an undamped oscillation at that frequency can already be observed when $G_c = 2.5$ radians. In any case, the fact that the oscillation occurs at about 2.8 Hz instead of the 3.5 Hz frequency that characterises the elastic mode indicates that the instability is related to the biomechanics of the pilot rather than to the elastic mode itself.

As a notable exception, pilot 2 did not show a PAO instability until quite a large value of G_c was reached while performing a slightly different task, which consisted of trying to maintain constant altitude using only the horizon as reference; the workload of this task is believed to be lower compared to

Table 4. Gearing ratio of LCO first appearance and corresponding frequency.

Case	Model		Pilot 1		Pilot 2		Pilot 3		Pilot 4	
	freq., Hz	Damp., %	freq., Hz	$G_c/G_{c_{\text{ref}}}$	freq., Hz	$G_c/G_{c_{\text{ref}}}$	freq., Hz	$G_c/G_{c_{\text{ref}}}$	freq., Hz	$G_c/G_{c_{\text{ref}}}$
Friction off										
12	5.80	34.9	3.95	∞[a]	3.8–4.0	∞	3.9–4.3	∞		
5	3.50	20.2	3.47	2.0	3.0	1.7	3.2	3.1	2.8	7.1
8	4.47	15.9	3.93	2.3	3.3	∞				
2	2.51	11.4	2.56	2.0	2.41	1.1–1.7	2.45	2.0	2.63	0.3
6	4.51	6.4	3.98	1.1	3.8	3.4				
11	5.94	12.0	4.50	∞						
10	5.97	6.0	4.05	4.0	3.8	5.1	4.7	∞		
9	5.98	4.2			3.85	6.9				
7	4.50	11.2			4.0	4.6	4.1	5.7		
Friction off, no close-in visual reference										
5	3.50	20.2			3.5–4.0	4.6–5.1				
Friction on										
1	2.53	4.3			4.1	3.1				
3	3.58	2.0			3.5	0.3				
4	3.57	4.0	3.5	2.3						

[a]∞ means that no instability was found.

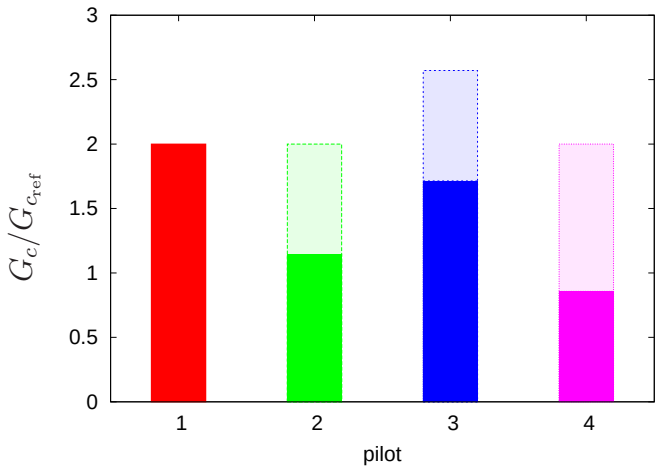

Fig. 17. Gearing ratios $G_c/G_{c_{\mathrm{ref}}}$ tested by all pilots with $k/k_{\mathrm{ref}} = 0.50$ and $c/c_{\mathrm{ref}} = 0.40$; shaded: highest tested value; solid: first observed instability.

that of the close-in visual references ADS-33 vertical manoeuvre. Significant dependence of the biomechanical response of the pilots on the task has already been verified in other biodynamic test campaigns (e.g. [24]).

4.4 Gearing Ratios with Reduced Elastic Mode Properties

Figure 17 shows the gearing ratios G_c experienced by different pilots in different test sessions using reduced values of both stiffness and damping, $k/k_{\mathrm{ref}} = 0.50$ and $c/c_{\mathrm{ref}} = 0.40$, for the elastic degree of freedom. As opposed to the previous case, non-professional pilots (1–3) showed a PAO instability at about 3.5 Hz for G_c values between 0.4 and 0.7 radians (above up to twice the reference value), while the professional pilot (4) encountered the instability at a lower value: at $G_c = 0.3$ radians considering the report of the pilot, but probably also at $G_c = 0.2$ radians according to the measured data. In this case the instability appeared at G_c values lower than nominal, meaning that if these particular model dynamics occurred in an actual rotorcraft whilst interacting with a pilot like pilot 4, then flight safety could be jeopardised.

In general, the rather different behaviour of the professional pilot (4), compared to the non-professional ones (1–3), can possibly be explained as follows. First, the professional pilot will have undergone more lengthy training and be more skilled in the task, which would explain the higher limit gearing ratio reached in Fig. 16. Second, he belonged to the 99th percentile in terms of height, thus probably showing somewhat different biomechanical properties to a more 'average' individual. This could explain the higher sensitivity to the elastic degree of freedom with reduced frequency showed in Fig. 17.

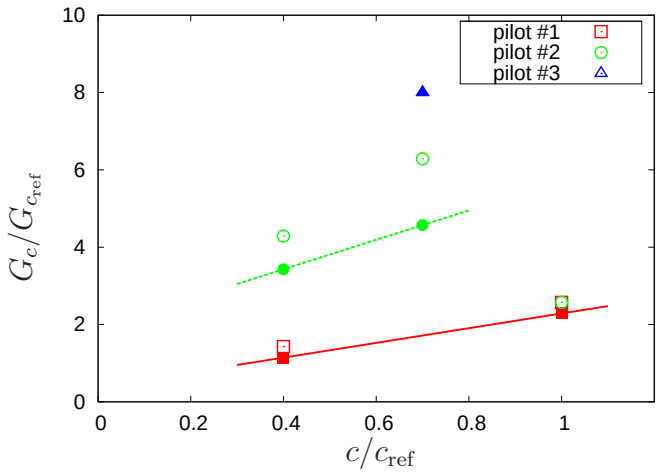

Fig. 18. Gearing ratios $G_c/G_{c_{\rm ref}}$ tested by all pilots with $k/k_{\rm ref} = 1.60$ and $c/c_{\rm ref} = 0.40, 0.70, 1.00$. Solid symbols indicate the first observed instability; empty symbols indicate the largest values tested.

4.5 Gearing Ratios with Increased Elastic Mode Frequency

Figure 18 shows the gearing ratios tested at $k/k_{\rm ref} = 1.60$ at different values of damping $c/c_{\rm ref}$ ranging between 0.40 and 1.00 (Cases #6, #7 and #8). Pilots 1 and 2 show a similar trend of gearing ratio with respect to the damping: as would be expected, they both require a larger gearing ratio when the damping is larger. However, the coupled system became unstable for pilot 2 at a gearing ratio more than twice that of pilot 1. It is worth noting that in the case at $c/c_{\rm ref} = 1.00$ the instability for pilot 1 occurred when an alarm was triggered, caused by a failure in the data acquisition system, which distracted the pilot. As a consequence, the instability in this specific case can be related to a sudden change in the pilot's attitude towards the task he was supposed to perform, i.e. a 'trigger' in the RPC sense [35].

A closer inspection of the data showed that pilot 3 may have unconsciously applied some strategy to limit the oscillations, since with $c/c_{\rm ref} = 0.7$ Limit Cycle Oscillations (LCO) were perceived only for $G_c \leq 2.8$ radians, although the data traces clearly show the onset of undamped oscillations starting at $G_c = 2.0$ radians.

4.6 Higher-Frequency Biomechanical Mode

Figure 19 shows the gearing ratios tested with $k/k_{\rm ref} = 2.80$ for different values of damping $c/c_{\rm ref}$ ranging between 0.35 and 1.00 (Cases #9, #10 and #11). This case was tested to ascertain whether a higher frequency pilot biomechanical mode at about 6 Hz could trigger an instability. The presence of a second

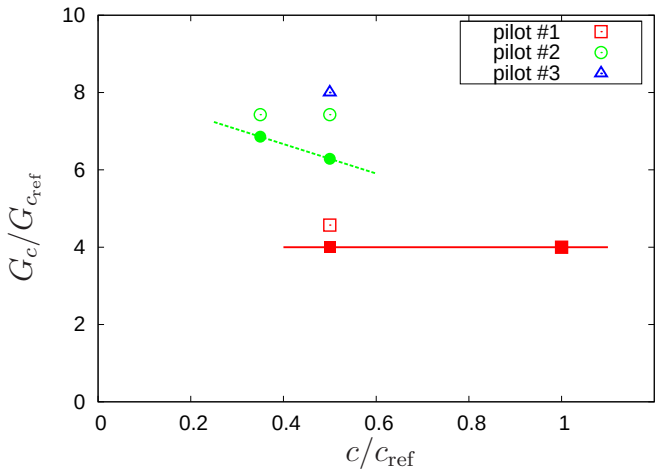

Fig. 19. Gearing ratios $G_c/G_{c_{\text{ref}}}$ tested by all pilots with $k/k_{\text{ref}} = 2.80$ and $c/c_{\text{ref}} = 0.35, 0.50, 1.00$. Solid symbols indicate the first observed instability; empty symbols indicate the largest values tested.

mode associated with vertical acceleration was noticed during a previous test campaign, described in Ref. [21], and indirectly observed during in-flight testing, as discussed in Ref. [22]. Pilots 1 and 2 required very large gearing ratios to yield a PAO. Pilot 3 could not reach a PAO. Again, significant variability was observed amongst the test subjects. A closer look at the oscillatory motion appearing in this case showed no evidence of a LCO in the vicinity of that frequency. On the contrary, all occurrences of undamped oscillations were observed at frequencies similar to those observed with structural properties tuned to yield lower frequencies, as reported in Table 4. This indicates that the oscillations were related to the fundamental biomechanical mode of the pilot, between 3.5 Hz and 4.0 Hz, rather than to the structural mode.

4.7 Collective Friction On

Table 4 also reports results related to tests performed with nominal friction in the collective control inceptor. Very small values of structural damping in the elastic mode were required to encounter a pilot-vehicle system instability for limited values of the gearing ratio. In both cases, with a nominally stiff elastic mode, the unstable oscillation occurred exactly at 3.5 Hz, the frequency of the elastic mode itself, while tests with nominal elastic properties and without friction resulted in unstable oscillations with a different frequency for each pilot, although quite close to 3.5 Hz. However, when the frequency of the elastic mode is moved below 3.5 Hz by halving the stiffness of the equivalent spring, the LCO appears at 4.1 Hz, a frequency that can only be associated with the biomechanics of the pilot (see Fig. 20(b)). This indicates that, even with collective friction on, the instability is associated with the biomechanical

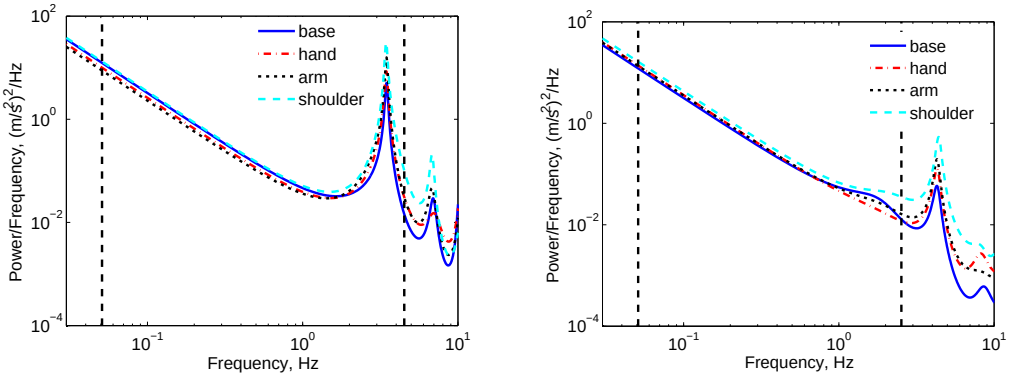

Fig. 20. Power spectral densities of the measured vertical accelerations of the pilot's limbs and of the motion base during an LCO with pilot 2; (a): $k/k_{\text{ref}} = 1.6$, $c/c_{\text{ref}} = 0.4$, friction off; (b): $k/k_{\text{ref}} = 0.5$, $c/c_{\text{ref}} = 0.15$, friction on. The vertical dashed lines indicate the poles of the 2DOF model.

properties of the pilot. The friction can thus be interpreted, in a quasi-linear dynamics sense, as an additional equivalent damping. As a consequence, it helps to reduce the phenomenon, but cannot prevent it in absolute terms.

It is also worth noting that without friction the second harmonic of the frequency that characterises the instability is always present and pronounced in the accelerations measured at the pilot's limbs (about 7.0 Hz in Fig. 20(a)). This indicates a quadratic nonlinearity in the behaviour of the coupled system. However, with nominal friction applied, such harmonics essentially disappear (Fig. 20(b)) possibly indicating that the presence of friction significantly modifies the mechanism that drives the PAO phenomenon.

5 Conclusions

This paper discussed an experimental activity conducted in the HELIFLIGHT simulation facility of the University of Liverpool within ARISTOTEL, a project sponsored by the European Community within the 7th Framework Programme. A simple model of the heave motion of a helicopter, including an elastic degree of freedom, was used as the flight mechanics model that provided motion demand to the motion base of the flight simulator. Closed-loop tests were performed, in which the collective control inceptor's rotation was fed into the simple flight mechanics model. Several configurations of the vehicle model and several variable parameters, specifically the gearing ratio between the collective control inceptor and the vertical force, and the frequency and amplitude of a disturbance force were tested using four human subjects, including a former military helicopter test pilot.

The experiments performed provided useful insight into the behaviour of human subjects coupled to the collective control layout and the dynamics of a rotary-wing vehicle. The interaction between the vertical oscillations of the helicopter and the involuntary rotation of the collective control represents a potential mechanism for Rotorcraft-Pilot Couplings. The placement of structural modes with frequencies in the vicinity of 2.5–4.0 Hz may result in an unstable interaction between the pilot and the vehicle. The presence of friction in the collective control inceptor may alleviate but not eliminate the phenomenon. When the frequency of the structural modes differs from that related to the biomechanics of the pilot, an instability is still possible, and it usually occurs at the frequency of the pilot's biomechanics. This is an indication that the structural dynamics can only amplify a phenomenon that is based on a mechanism directly related to the presence of the human operator.

The experimental tests showed a significant inter- and intra-subject variability. Different subjects reached the boundary of stability for different values of the gearing ratio, and occasionally the same subject reached an instability for different values of the gearing ratio in sensibly identical test conditions. The biomechanical response of the pilots also showed some dependence on the task. In some cases the subject could recover from instability by changing the control strategy, e.g. by starting a manoeuvre. Replacing the precision task with a nominally lower pilot gain task resulted in larger limit gearing ratios for the same subject and vehicle model.

The biodynamic feedthrough model provided by Mayo's transfer functions appeared to be overly conservative, since in the experiments the stability limit was usually reached with gearing ratios at least as large as twice the nominal value predicted using Mayo's functions.

Devising means to prevent adverse involuntary couplings is outside the scope of the present work. However, it is clear from this work that a force control mechanism that produces changes in vertical force as a consequence of (nearly) vertical motion of the forearm, specifically producing force when moving opposite to the force direction, is intrinsically prone to adverse coupling with the biomechanics of the pilot.

Acknowledgements

The support of Mr. Michael Jones in the execution of the tests is gratefully acknowledged. The research leading to these results has received funding from the European Community's Seventh Framework Programme (FP7/2007–2013) under grant agreement N. 266073. The European Community, as the funding source, had no role in the design of the study, in the collection, analysis and

interpretation of data, in the writing of the report, and in the decision to submit the article for publication.

References

[1] M. D. Pavel, M. Jump, B. Dang-Vu, P. Masarati, M. Gennaretti, A. Ionita, L. Zaichik, H. Smaili, G. Quaranta, D. Yilmaz, M. Jones, J. Serafini, J. Malecki, Adverse rotorcraft pilot couplings — past, present and future challenges, Progress in Aerospace Sciences (in press, available online 4 July 2013), doi:10.1016/j.paerosci.2013.04.003.

[2] M. D. Pavel, J. Malecki, B. DangVu, P. Masarati, M. Gennaretti, M. Jump, M. Jones, H. Smaili, A. Ionita, L. Zaicek, Present and future trends in aircraft and rotorcraft pilot couplings — a retrospective survey of recent research activities within the European project ARISTOTEL, in: 37th European Rotorcraft Forum, Gallarate, Italy, 2011, Paper no. 116.

[3] M. D. Pavel, J. Malecki, B. DangVu, P. Masarati, M. Gennaretti, M. Jump, H. Smaili, A. Ionita, L. Zaicek, A retrospective survey of adverse rotorcraft pilot couplings in European perspective, in: American Helicopter Society 68th Annual Forum, Fort Worth, Texas, 2012.

[4] O. Dieterich, J. Götz, B. DangVu, H. Haverdings, P. Masarati, M. D. Pavel, M. Jump, M. Gennaretti, Adverse rotorcraft-pilot coupling: Recent research activities in Europe, in: 34th European Rotorcraft Forum, Liverpool, UK, 2008.

[5] R. W. Prouty, A. R. Yackle, The Lockheed AH-56 Cheyenne — Lessons learned, in: AIAA Aircraft Design Systems Meeting, Hilton Head, SC, USA, 1992, AIAA-1992-4278.

[6] T. Parham, Jr., D. Popelka, D. G. Miller, A. T. Froebel, V-22 pilot-in-the-loop aeroelastic stability analysis, in: American Helicopter Society 47th Annual Forum, Phoenix, Arizona (USA), 1991.

[7] R. B. Walden, A retrospective survey of pilot-structural coupling instabilities in naval rotorcraft, in: American Helicopter Society 63rd Annual Forum, Virginia Beach, VA, 2007, pp. 1783–1800.

[8] M. Gennaretti, J. Serafini, P. Masarati, G. Quaranta, Effects of biodynamic feedthrough in rotorcraft-pilot coupling: Collective bounce case, J. of Guidance, Control, and Dynamics, (in press, available online 25 July 2013), doi:10.2514/1.61355.

[9] J. Serafini, M. Gennaretti, P. Masarati, G. Quaranta, O. Dieterich, Aeroelastic and biodynamic modeling for stability analysis of rotorcraft-pilot coupling phenomena, in: 34th European Rotorcraft Forum, Liverpool, UK, 2008.

[10] P. Masarati, G. Quaranta, M. Gennaretti, J. Serafini, Aeroservoelastic analysis of rotorcraft-pilot coupling: a parametric study, in: American Helicopter Society 66th Annual Forum, Phoenix, AZ, 2010.

[11] D. T. McRuer, H. R. Jex, A review of quasi-linear pilot models, Human Factors in Electronics, IEEE Transactions on HFE-8 (3) (1967) 231–249, doi:10.1109/THFE.1967.234304.

[12] R. E. Magdaleno, D. T. McRuer, Effects of manipulator restraints on human operator performance, Air Force Flight Dynamics Laboratory Tech. Rep. 66-72 (1966).

[13] D. T. McRuer, R. E. Magdaleno, Human pilot dynamics with various manipulators, Air Force Flight Dynamics Laboratory Tech. Rep. 66-138 (1966).

[14] R. W. Allen, H. R. Jex, R. E. Magdaleno, Manual control performance and dynamic response during sinusoidal vibration, Aerospace Medical Research Laboratory Tech. Rep. 73-78 (October 1973).

[15] H. R. Jex, R. E. Magdaleno, Biomechanical models for vibration feedthrough to hands and head for a semisupine pilot, Aviation, Space, and Environmental Medicine 49 (1–2) (1978) 304–316.

[16] R. W. McLeod, M. J. Griffin, Review of the effects of translational whole-body vibration on continuous manual control performance, Journal of Sound and Vibration 133 (1) (1989) 55–115, doi:10.1016/0022-460X(89)90985-1.

[17] S. J. Merhav, M. Idan, Effects of biodynamic coupling on the human operator model, J. of Guidance, Control, and Dynamics 13 (4) (1990) 630–637, doi:10.2514/3.25380.

[18] D. G. Mitchell, B. L. Aponso, D. H. Klyde, Effects of cockpit lateral stick characteristics on handling qualities and pilot dynamics, CR 4443, NASA (1992).

[19] Anonymous, Rotorcraft flying handbook, FAA H-8083-21, Federal Aviation Administration (2000).

[20] J. R. Mayo, The involuntary participation of a human pilot in a helicopter collective control loop, in: 15th European Rotorcraft Forum, Amsterdam, The Netherlands, 1989, pp. 81.1–12.

[21] P. Masarati, G. Quaranta, M. Jump, Experimental and numerical helicopter pilot characterization for aeroelastic rotorcraft-pilot couplings analysis, Proc. IMechE, Part G: J. Aerospace Engineering 227 (1) (2013) 124–140, doi:10.1177/0954410011427662.

[22] P. Masarati, G. Quaranta, W. Basso, R. Bianco-Mengotti, C. Monteggia, Preliminary in-flight biomechanic tests on the BA-609 fly-by-wire tiltrotor, in: 21st Society of Flight Test Engineers, European Chapter Symposium, Vergiate (VA), Italy, 2010.

[23] M. Jump, S. Hodge, B. DangVu, P. Masarati, G. Quaranta, M. Mattaboni, M. D. Pavel, O. Dieterich, Adverse rotorcraft-pilot coupling: Test campaign development at the university of Liverpool, in: 34th European Rotorcraft Forum, Liverpool, UK, 2008.

[24] J. Venrooij, D. Yilmaz, M. D. Pavel, G. Quaranta, M. Jump, M. Mulder, Measuring biodynamic feedthrough in helicopters, in: 37th European Rotorcraft Forum, Gallarate, Italy, 2011, pp. 199.1–12.

[25] G. D. Padfield, M. D. White, Flight simulation in academia; HELIFLIGHT in its first year of operation, The Aeronautical Journal of the Royal Aeronautical Society 107 (1075) (2003) 529–538.

[26] G. D. Padfield, Helicopter Flight Dynamics: The Theory and Application of Flying Qualities and Simulation Modelling, Blackwell Publishing, 2007.

[27] J. Venrooij, D. A. Abbink, M. Mulder, M. M. van Paassen, M. Mulder, Biodynamic feedthrough is task dependent, in: 2010 IEEE International Conference on Systems Man and Cybernetics (SMC), Istanbul, Turkey, 2010, pp. 2571–2578, doi:10.1109/ICSMC.2010.5641915.

[28] P. Masarati, G. Quaranta, L. Zaichik, Y. Yashin, P. Desyatnik, M. D. Pavel, J. Venrooij, H. Smaili, Biodynamic pilot modelling for aeroelastic A/RPC, in: 39th European Rotorcraft Forum, Moskow, Russia, 2013.

[29] P. Masarati, G. Quaranta, A. Zanoni, Dependence of helicopter pilots' biodynamic feedthrough on upper limbs' muscular activation patterns, Proc. IMechE Part K: J. Multi-body Dynamics (in press, available online 1 July 2013), doi:10.1177/1464419313490680.

[30] G. Quaranta, P. Masarati, J. Venrooij, Impact of pilots' biodynamic feedthrough on rotorcraft by robust stability, Journal of Sound and Vibration 332 (20) (2013) 4948–4962, doi:10.1016/j.jsv.2013.04.020.

[31] G. Quaranta, A. Tamer, V. Muscarello, P. Masarati, M. Gennaretti, J. Serafini, M. M. Colella, Rotorcraft aeroelastic stability using robust analysis, CEAS Aeronaut. J., doi:10.1007/s13272-013-0082-z.

[32] S. Skogestad, I. Postlethwaite, Multivariable Feedback Control, John Wiley & Sons, Chichester, 2005.

[33] Anonymous, Performance specification, handling qualities requirements for military rotorcraft, ADS 33-E-PRF, US Army AMCOM, Redstone, Alabama (2000).

[34] M. J. Griffin, Handbook of Human Vibration, Academic Press, London, 1990.

[35] D. T. McRuer, Aviation Safety and Pilot Control: Understanding and Preventing Unfavourable Pilot-Vehicle Interactions, Washington DC: National Research Council, National Academy Press, 1997.

List of Figures

List of Tables